UNIVERSITY OF THESSALY

DEPARTMENT OF MECHANICAL ENGINEERING

DIPLOMA THESIS

Precipitation and hardening during homogenization cooling of aluminum alloys

By

Fanikos Ioannis

Thesis supervisor: Prof. G.N. Haidemenopoulos

Submitted for the partial fulfillment
of the requirements for obtaining
the Diploma of Mechanical Engineering

2017

Approved by the examination committee

First Examiner   Dr. G. N. Haidemenopoulos
(Supervisor)   Professor, Department of Mechanical Engineering, University of Thessaly

Second Examiner   Dr. N. Aravas
Professor, Department of Mechanical Engineering, University of Thessaly

Third Examiner   Dr. A. Kermanidis
Assistant Professor, Department of Mechanical Engineering, University of Thessaly

Acknowledgements

I would like to thank Professor G.N. Haidemenopoulos for his guidance, patience and support throughout our collaboration on this thesis and throughout my studies. I would also like to thank the other members of the examination committee, Professor N. Aravas and assistant Professor A. Kermanidis for their careful reading of my thesis. I would like to thank the staff of the laboratory of materials of the University of Thessaly but especially Dr. Panagiota Sarafoglou who never left any of my questions unanswered and who provided the materials necessary for the experimental validation of my thesis. I would like to thank Alexandros Serafeim for his help with all the problems I ran into during the writing of my thesis. I would like to thank Margianna Tzini for the aid that she provided with the magnesium equilibrium concentration equation. I would like to thank Paraskevi Stavraki for her patience and support throughout the last months of writing this thesis and my friend John Oksuzoglou for his moral support. Finally I would like to express my gratitude to my parents Asterios and Chrysoula Fanikos for their love and support throughout all these years.

1. Summary

The mechanical properties required for the applications of the 6xxx series aluminium alloys are obtained by the precipitation of the intermetallic phase Mg_2Si. The microstructure that occurs is responsible for the mechanical properties of the alloy. So if the microstructure can be predicted (precipitate volume fraction, size), the final mechanical properties can be predicted as well. This prediction can be achieved by the application of the kinetic model Kampmann & Wagner (KWN), which takes into account all the diffusion mechanisms that occur during an isothermal process. During an isothermal process, nucleation, growth and coarsening take place at the same time, in different speeds depending on the time that has passed since the beginning of the thermal process. The model uses the population balance equation (PBE) in the solid state which includes the nucleation and growth parameters. Coarsening occurs naturally without any additional parameters. The semi-discretization numerical method is used in the model used to solve the equation. Equations describing the rate of nucleation and growth were developed and inserted in the PBE. Through additional steps that are further described later, the model was configured in order to simulate non-isothermal processes. This allows us to configure the thermal process in order to achieve the properties required for every application without the need for experimentation which is very important in the alloy engineering science. The model was applied on three aluminum alloys (6005, 6063, 6082) in order to predict the yield strength after the process of homogenization and cooling.

Table of Contents

List of Figures

List of Tables

2. Introduction

The 6000 series aluminum alloys, are very popular for shaping through extrusion because of their good extrudability and final mechanical properties. This is a result of the alloy's microstructure before, during and after the process. These alloys contain magnesium and silicon as major alloying elements which produce the compound Mg_2Si. This compound provides the alloy's heat-treatability. An industrial extrusion process typically starts with the casting of the billet. Then the billet is homogenized in order to dissolve the Mg_2Si. The properties of the billet after the homogenization and cooling procedure is crucial to the extruding process, but experimental determination of the homogenization and cooling parameters can be expensive and inefficient. On the other hand, a simulation of the process and the final properties, can save both resources and time.

Homogenization comprises of three major steps, heating the as-cast billet with a particular rate, holding at a constant temperature for a certain time, and cooling with a proper cooling rate. Cooling of the billet after homogenization is very important in order to obtain the suitable microstructure to improve extrudability as well as the final mechanical properties of the extrusion [1]. A fully solutionized billet, as obtained at the end of homogenization holding, is difficult to extrude due to solid solution strengthening. The motivation behind controlled cooling is the establishment of a specific precipitation state [2]. During cooling to room temperature precipitation of Mg_2Si and other Fe, Mn and Cr containing phases takes place. The size and the density of these particles are crucial because they enhance the recrystallization resistance of the material [2], which is beneficial for the final mechanical properties. Respectively, the size and the density of Mg_2Si particles must be such that they can be dissolved easily before extrusion, leading to improved extrudability [3]. It has been shown that smaller Mg_2Si particles, obtained after cooling, dissolve faster during extrusion [2-4]. The amount of Mg and Si in solid solution, and hence the amount of Mg_2Si precipitated, are highly affected by the cooling rate from the homogenization temperature.

Slow cooling tends to produce coarse Mg_2Si particles while rapid cooling trap the Mg and Si in solution with little or no Mg_2Si precipitation [5,6]. A decrease in the cooling rate increases the Mg_2Si precipitation and decreases the amount of Mg in solid solution. Zajac et al. [3] and Nowotnik et al. [7], investigated the effect of the cooling rate on the final mechanical properties of the 6005, 6082 and 6063 aluminum alloys. Usta et al. [8] and Van de Langkruis [4,9] studied the dissolution-coarsening kinetics of the Mg2Si particles during reheating. Reiso et al. [5] correlated the cooling rate to the maximum extrusion velocity for various chemical compositions of AlMgSi alloys. Birol et al. [10,11] studied the effect of the homogenization temperature, time and cooling rate on the microstructure of 6063 and 6082 alloys through metallographic techniques. Priya et al. also simulated the post-homogenizing quenching of aluminium alloys using the model of Myhr and Grong and noticed two nucleation events. The first one occurred at 400-420C and the second one around 200-320C [12]. As mentioned

above, most of the published work approaches the homogenization process experimentally. The modelling or simulation work is rather limited.

The billet is kept at a high temperature during the extrusion process in order to avoid any precipitation of Mg_2Si particles. As mentioned before the final product's properties depend largely on the alloys microstructure and specifically on the Mg_2Si precipitates. That's why after the extrusion, further process is necessary in order to achieve the properties desired. The process of ageing follows, where the billet is heated at a predetermined temperature for a period of time. During that process, particles of Mg_2Si precipitate and give the alloy it's final properties. The final strengthening of the alloy depends greatly on the temperature and duration of the ageing. Ageing at higher temperature produces an earlier but lower peak hardness compared with ageing at the lower temperature.

The precipitation sequence for 6XXX alloys, which is generally accepted in the literature, is

$$SSSS \Rightarrow \text{atomic clusters} \Rightarrow \text{GP zones} \Rightarrow \beta'' \Rightarrow \beta' \Rightarrow \beta \text{ (stable)}$$

The β'' precipitate is associated with peak-aged conditions, is needle shaped and aligned along $<100>_{Al}$ with a composition of Mg_5Si_6. They range between 200 and 1000 Å in length and are ≈60 Å in diameter. This precipitate is the predominant precipitate in peak-aged alloys and makes the most contribution in strengthening the alloy.   B' precipitates form after β'' precipitates in the ageing sequence. They are rod shaped and are aligned along $<100>_{Al}$ with the hexagonal structure of a=7.05 A and c=4.05A. Through energy dispersive spectroscopy β' phase is said to obtain an Mg:Si ration of 1.68. The equilibrium Mg_2Si phase, which is formed last, forms as platelets lying in $\{100\}_{Al}$ planes. The structure has been well characterized as the FCC anti-fluorite structure with a = 6.39 Å. This precipitate contributes less to the strength of Al-Mg-Si [13]

As stated before, precipitation strengthening is the main strengthening mechanism for the aluminium alloys of the 6xxx series, which is achieved through artificial ageing. Throughout the process of artificial ageing phase transformations take place that include nucleation, growth and coarsening. The above mentioned mechanisms act simultaneously throughout the whole process. Nevertheless the process can be subcategorized in three parts. In the first part, the most dominant mechanism is nucleation. In this time period the nucleus in the matrix are created under the influence of the driving force for nucleation which depends on supersaturation and temperature. These nuclei then begin to grow by the diffusion of the alloying elements from the matrix to the nuclei, which results in a reduction of the supersaturation and consequently in a reduction of the driving force. In the second part of the process, the volume fraction of the precipitants approach the value of the thermodynamic equilibrium. Here the dominant mechanism is growth. The third part of the process, begins as soon as the volume fraction of the precipitants reaches the value indicated in the phase diagram. The volume fraction of the precipitated particles stay constant while components diffuse from the smaller to the larger particles. As a result, the number of particles decrease while their size increase. The above processes result in a dispersion of precipitates in the

matrix which can be described by a particle size distribution. This distribution is a result from the solution of the PBE by taking into account simultaneous nucleation growth and coarsening and by making some simplifying assumptions. The most basic assumption is that the infinite dilution model is considered, which means that the diffusion of the alloying elements towards a nucleus is not affected by the diffusion in the neighboring nucleus. This assumption makes possible, the solution of the diffusion equation for a partible in an infinite matrix.

In the field of phase transformation with nucleation, growth and coarsening in isothermal and non-isothermal processes, few are the models that have been suggested in order to describe the distribution of particles where nucleation growth and coarsening occurred simultaneously. Initially Lifshitz & Slyozov [14] studied the growth and coarsening of particles in solid state by using the PBE in order to predict the particle distribution, by assuming that they were formed according to the mechanism of continuing transformations and not by the classical theory of nucleation. Langer & Schwartz also studied the nucleation and growth of drops for the purpose of calculating the time needed for two mixtures to be separated. Wagner & Kampmann [15] were the first to suggest a numerical model that took into account simultaneous action of all three mechanisms. Myhr & Grong [16] modified the KWN model to be applied using finite elements methods in order to predict the distribution of particles during ageing of aluminum alloys [17] as well as for the development of the microstructure in the heat affected zone of welded joints [18]. Robson et.al used the KWN model to calculate the particle distribution during precipitation in Al-Zr alloys as well as to identify the effect of Sc on the number of the particles in Al-Zr-Sc alloys [19]. They also used the KWN model to study the effect of other parameters (diffusion coefficient, supersaturation, interfacial energy) on the distribution of particles [20]. Finally, the KWN model was widely used in FSW [21], where it is applied along a thermal model or an additional phase transformation model so that the final mechanical properties can be calculated.

In the present study, emphasis was given on the KWN model in order to calculate the particle distribution in non-isothermal processes (cooling after homogenization) of the 6061, 6005, 6063 aluminum alloys. The prediction of the microstructure and properties of the alloy after homogenization and cooling is the aim of this study. The nucleation rate was calculated using a time dependent model based on the Bocker-Doring theory. The nucleation/dilution rate was calculated by solving the diffusion equation in isothermal conditions and assuming constant rate of nucleation. The Gibbs-Thomson equation was included in the model in order for coarsening to be included too. Finally the diffusion coefficient was considered independent of concentration and that diffusion is controlled only by magnesium.

3. Methodology

3.1 Methodology - Computational

As mentioned before, the purpose of the simulation is the calculation of the particle distribution. For that reason, the PBE will be used which contains the parameters for nucleation and growth. For the simulations, three aluminum alloys were chosen, 6082, 6063 and 6005, whose composition is stated below.

Alloy	Al	Si	Fe	Cu	Mn	Mg
6063	98.79	0.4194	0.1895	0.0012	0.0311	0.5346
6005	98.29	0.686	0.1552	0.1106	0.2227	0.4896
6082	97.82	0.9	0.2	-	0.45	0.63

Table 1: Alloys Composition

The main assumptions that were made during the development of the model are:

- Diffusional phase transformation
- Constant diffusion coefficients
- Process is controlled by Mg diffusion
- Interactions of magnesium with other elements are ignored
- Infinite dilution of the matrix
- Spherical particles
- Stoichiometric particle composition
- Diffusion fields around the particles do not cross

3.1.1 Population Balance Equation (PBE)

In many problems, multiphase systems with distributed particle phases, need to be described [**22, 23**]. The objective is to predict the distribution of one or more properties of the material. The population balance equation essentially is a preservation principle of the quantity of these properties by describing their time dependence. In this particular case, the property we are studying is the particle diameter. So the particle balance equation takes the following form

$$\frac{\partial n(D,t)}{\partial t} + \frac{\partial [G(D,t)n(D,t)]}{\partial D} = \delta \bullet (D - D^*) \bullet S(t)$$

Initial Condition $n(D,0) = 0$

Boundary Conditions $n(0,t) = 0$

$n(\infty,t) = 0$

Where n(D,t) represent the number of particles of a certain diameter $[\#/m]$, G(D,t) is the growth/dilution rate $[m/s]$ and S(t) is the nucleation rate $[\#/m^3]$.

Since n(D,t) describes a distribution, the distribution's moments have to be described as well.

Order	Definition	Physical meaning
0-order	$\mu_0 = \int\limits_0^\infty n(D,t)dD$	Number of particles
1st-order	$\mu_1 = \int\limits_0^\infty Dn(D,t)dD$	Sum of particle diameters
2nd-order	$\mu_2 = \int\limits_0^\infty D^2 n(D,t)dD$	Sum of particle surfaces
3rd-order	$\mu_3 = \int\limits_0^\infty D^3 n(D,t)dD$	Volume fraction

Table 2: Moment Definition

The definitions mentioned above have a very specific natural meaning and through them we obtain information about the distribution of the particles.

Total number of particles: $N=\mu_0$

Volume fraction of particles: $f=\mu_3$

Mean particle diameter: $\bar{D} = \dfrac{\mu_1}{\mu_0}$

3.1.2 Nucleation

Nucleation is a process during which the smallest possible particle of the new phase is created, called the nuclei. Before the actual nucleation, there is a particle called embryo which is even smaller than the critical radius needed for nucleation. This particle gradually grows through rejecting and receiving atoms. According to the mobility theory, not all embryos turn into nuclei. Most of them dilute back into the matrix due to thermal variances near the area of the critical radius. Even particles larger than the critical radius may be diluted back into the matrix. Therefore, the nucleation rate should take into consideration the incubation period, which is the time necessary to create a stable nucleus according to Becker-During [24]. By solving the second Fick Law for nucleus concentration in the matrix and the rate of atom inflow inside the nucleus as diffusion coefficient, the following equation occurs:

$$S(t) = N_0 Z \beta^* \exp(-\frac{\Delta G^*}{kT}) \exp(-\frac{\tau}{t})$$

Where N_0 is the number of homogeneous and heterogeneous nucleation sites, Z is the Zeldovich number through which the thermal variation near the critical radius area [24], can be considered. K is the Boltzmann constant, β^* is the rate of atoms' inflow inside the nucleus and is given by the following equation

$$\beta^* = \frac{4\pi R^{*2} D\, C_0}{a^4}$$

R* is the critical radius for nucleation, α is the lattice constant, D is the diffusion coefficient and C_0 is the nominal composition of the alloy. DG* is the energy barrier for nucleation and is given by the following equation:

$$\Delta G^* = \frac{\Delta G_0}{\ln^2\left(\bar{C}/C_{eq}\right)}$$

DG₀ is an adjustable variable that includes all the parameters that constitute the energy barrier (thermodynamic and mechanic). The symbol τ represents the incubation period, which adds the time needed to achieve the proper conditions for nucleation, in the equation of nucleation

$$\tau = \frac{1}{2\beta^* Z^2}$$

The Gibbs-Thomson equation is solved in order to calculate the critical radius for nucleation for $C_i = \bar{C}$:

$$C_i = C_{eq} \exp\left(\frac{2\gamma V_m}{rRT}\right)$$

$$r^* = \frac{2\gamma V_m}{RT}\left(\ln\left(\frac{\bar{C}}{C_{eq}}\right)\right)^{-1}$$

$\bar{C}$ is the mean element concentration in the matrix, γ is the interfacial energy, V_m is the molecular volume of the precipitate and C_{eq} is the equilibrium concentration. As mentioned in the assumption that were made, all the concentrations refer to magnesium. The equilibrium concentration is given by the phase diagram for the Mg₂Si phase [18]:

$$C_{eq}(\%) = 970\exp(\frac{-Q_0}{R*T})$$

Where Qs is the solvus energy.

3.1.3 Growth

For the calculation of the growth rate, the following assumptions are made: a) infinite dilution b) diffusion is controlled by magnesium. Along with the assumptions that the diffusion coefficient and temperature are stable, the diffusion equation is solved [25]

$$\frac{dC}{dt} = \frac{D}{r^2}\frac{d}{dr}(r^2\frac{dC}{dr})$$

Initial Condition $c(r,0) = \bar{C}$

Boundary Conditions $c(r,t) = C_i$

$$c(\infty,t) = \bar{C}$$

$$G = \frac{\bar{C}-C_i}{C_p-C_i}\frac{D}{r}$$

Ci is given by the Gibbs-Thomson equation. According to the Gibbs-Thomson equation for the critical radius, all particles with r<r$_c$ are supposed to dilute while the rest should grow.

The concentration of the matrix can be calculated using a simple mass balance equation

$$\bar{C} = \frac{C_0 - f \bullet C_p}{1-f}$$

3.1.4 Numerical Model

The calculations are impossible to be performed analytically so the must be performed numerically by using the method of semi-discretization. According to this method a partial differential equation of two variables, is discretized only on one direction (space) [26]. As a result, a system of normal differential equations occur that are dependent only to time. In this particular case, the variable of diameter is discretized. Considering that e parts of discretization are chosen, we transform the PBE in an e_xe system of equations with e unknown variables. More specifically:

$$\frac{\partial N_i}{\partial t} = -G(D,t)n(D,t)\big|_{D_{i+1}} + G(D,t)n(D,t)\big|_{Di} + \delta_{ij}S(t)$$

Kronecker's delta function defines that the nucleation occurs at the j element which is the one where the critical nucleus size D* belongs.

In order for this system to be solved, the values of [n(D,t)G(D,t)] at the interval boundaries are required.

$$n(D,t)G(D,t)\big|_{d_i} = \frac{N_{i-1}}{h}G(D_i,t) \qquad \text{Growth: } G(D_i,t) > 0$$

$$n(D,t)G(D,t)\big|_{d_i} = \frac{N_i}{h}G(D_i,t) \qquad \text{Dilution: } G(D_i,t) < 0$$

For dilution PBE has the following form

$$\frac{dN_i}{dt} = -\frac{N_{i+1}}{h}G(D_{i+1},t) + \frac{N_i}{h}G(D_i,t)$$

The parameter of nucleation is obviously zero in case of dilution.

3.1.5 Non-Isothermal Processes

The model has also been used in non-isothermal processes [**17,18,21**]. In literature the problem of microstructure prediction in non-isothermal processes, is approached by models that calculate the probable dilution and coarsening at the end of the process without calculating the particle distribution and the mean radius during the process. In the present study, an attempt has been made in order to calculate the particle distribution during the whole thermal cycle. A popular method of converting between isothermal and non-isothermal transformation data is the additive reaction rule of Scheil [**30**]. A cooling curve is treated as a combination of a sufficiently large number of isothermal reaction steps. This has been achieved by discretizing the thermal cycle into many isothermal cycles, as shown in figure 1.
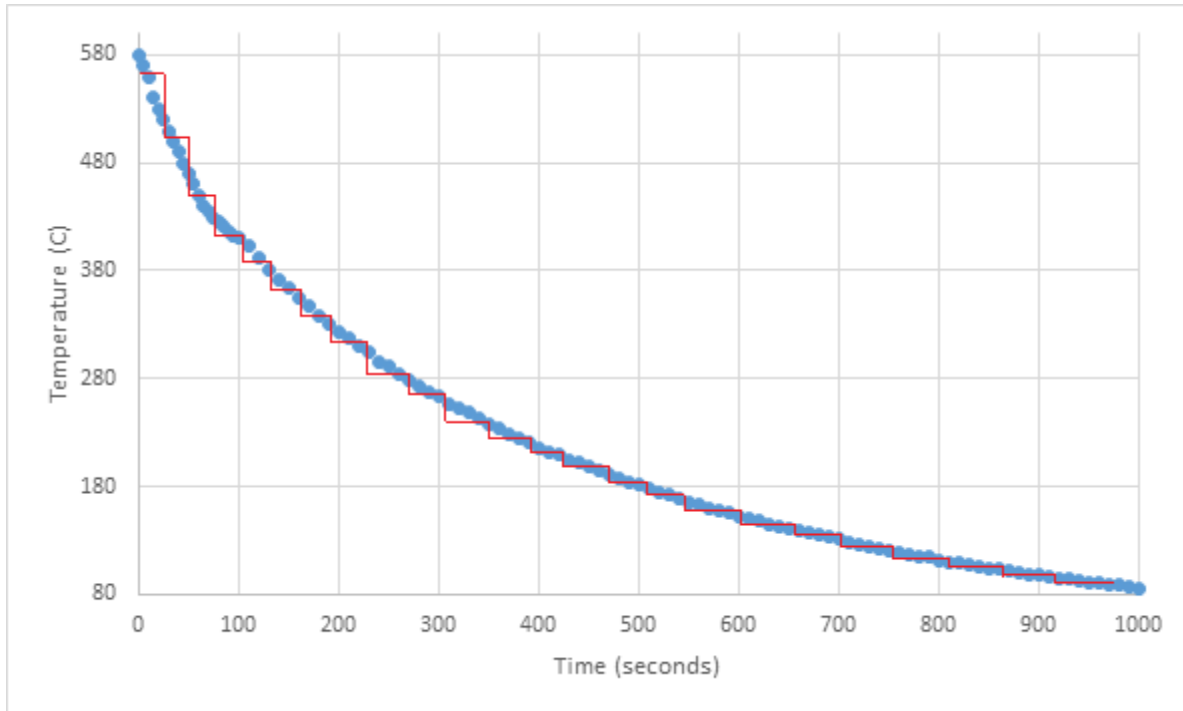
Figure 1: Thermal cycle discretization

In every isothermal part of the thermal cycle, thermodynamic equilibrium is considered and the model is applied for a time defined by the size of the discretization. This way, a solution for every part of the cycle is calculated and the results are used in order to calculate the results of the next part of the cycle.

3.1.6 Precipitation hardening model

The total hardening in the heat hardened alloys, is a result of five different mechanisms: work hardening σ_{WH}, Hall-Petch hardening σ_{GB}, lattice resistance hardening σ_I, solid solution hardening σ_{ss} and precipitation hardening σ_p. This model's purpose is to describe the alteration of the yield strength (or hardness) of aluminum alloys during thermal processes, by taking into consideration the particle size distribution, the volume fraction as well as the particles mean radius [27]. The total yield strength is given by the following equation:

$$\sigma = \sigma_I + \sigma_{WH} + \sigma_{GB} + \sigma_{SS} + \sigma_P$$

Solid solution strengthening depends on the mean concentration of each element in the matrix and is calculated by the equation [28]:

15

$$\sigma_{ss} = \sum K_j \bar{C}_j$$

Precipitation hardening depends on the mean obstacle strength F and can be calculated by the following equation [16,21,29]

$$\sigma_P = \frac{M\bar{F}}{bl} F$$

M is the Taylor factor, b is the magnitude of burgers vector and l is the particle spacing along a bending dislocation.

The mean obstacle strength depends on whereas the particle is shearable or not. If the particle is shearable (r<r_{sh}), then F depends on the particle's diameter [29]:

$$F_i = 2\beta G b^2 \frac{r_i}{r_{sh}}$$

If the particle is not shearable (r>r_{sh}) then the mean obstacle strength is given by the following equation:

$$F_i = 2\beta G b^2$$

Where r_{sh} is the critical shear radius.

In case that the population of the particles consists of both shearable and non-shearable particles then the mean obstacle strength is given by:

$$F = \frac{\int_0^\infty n(D,t)F(D)dD}{\int_0^\infty n(D,t)dD} = \frac{\sum_{i=1}^k N_i F_i}{\sum_{i=1}^k N_i}$$

Where k_p is defined as:

$$K_p = 2\beta G b M \sqrt{\frac{3}{2\pi}}$$

For particles with r<r_{sh}

$$\sigma_p = k_p \frac{\sqrt{f}}{\bar{r}} \left(\frac{\sum\limits_{i=1}^{k} N_i F_i}{\sum\limits_{i=1}^{k} N_i} \right)^{\frac{3}{2}}$$

While for particles with $r > r_{sh}$

$$\sigma_p = k_p \frac{\sqrt{f}}{\bar{r}}$$

The above equations allow the prediction of the time dependent variation of the yield strength through the volume fraction f and the mean radius $\bar{r}$. It is worth mentioning that all the parameters included in the calculation of the yield strength are treated as calibration variables, whose values are determined by experimental data [28].

3.1.7 Application of the model on the 6063 6005 6082 alloys

For the verification of the simulation, the results are compared to the experimental results. The experimental procedure is analyzed in the next paragraph. The values of the variables for the simulation are listed in the table below:

Parameter	Value	Description	Reference
Cp (% wt)	63.4	Concentration of magnesium in Mg_2Si	(5)
A (m)	4.04×10^{-10}	Lattice constant	(13)
D0 (m^2/s)	2.02×10^{-4}	Pre-exponential parameter of diffusion coefficient	(5)
Q0 (J/mol)	130000	Diffusion activation energy	(5)
k	1.38×10^{-23}	Boltzmann constant	
R(j/molK)	8.314	Global gas constant	
γ (J/m^2)	0.5	Interfacial energy	(19)
Vm	3.84×10^{-5}	Molecular volume	(19)
N0	2×10^{20}	Nucleation points	Adjustable variable
DG0	1.01×10^{-19}		(21)
r_c	5×10^{-9}	Critical shear radius	(4)
σ_0 (MPa)	70	Constant parameter	(4) (11)

		in the hardening model	
K_{si}	66.3	Solid solution strengthening of silicon parameter	(4) (11)
K_{mg}	29	Solid solution strengthening of magnesium parameter	(4) (11)
K_{ppt}	$4x10^{-6}$	Precipitation strengthening parameter	(5)

Table 3: Simulation Variable Values

There is a lack of values for variables concerning the microstructure (interfacial energy of the precipitates of the matrix, thermodynamic data of metastable phases, density of nucleation sites, driving force for nucleation) and the interaction of the dislocations with the microstructure. For that reason, approximate values were used. As for thermodynamic data, simple models were used in order to calculate their values. Nevertheless, this lack of specific values for these parameters, have led the researchers to different techniques in order to predict the evolution of the microstructure during thermal processes.

- Use of experimental data for the description of the evolution of the microstructure. Myhr& Grong used experimental toughness data in order to describe the decrease of toughness in aluminum alloys welds.
- Documentation of the evolution of the microstructure, adjustment of known equations like the Jonshon-Mehl-Avrami equation for the volume fraction and finally the calibration of the mechanical properties models using experimental data

In this particular model, three adjustable variables were considered: N_0, Dg_0 and k_{ppt}. The values of these variables are determined by experimental data taken either from the experiments of this study or literature as well as from the LSW theory.

3.2 Methodology - Experimental procedures

3.2.1 Materials

As mentioned before, the KWN model, through the prediction of the microstructure, is able to predict the variation of the yield strength throughout the process. A series of tensile tests were made on the already mentioned three aluminum alloys (6082, 6063, 6005) in order to verify the results of the simulation. The received billets were sectioned in transverse slices as shown in Fig. 2. The samples were cut from approximately the middle of the billet's slice radius in order to avoid edge inhomogeneities and other casting defects.

Figure 2: Specimen raw material

3.2.2 Heat Treatment

The dimensions of each section was 14cm x 2cm x 2cm as shows in Fig. 3. A hole of 1cm in diameter was drilled in one of the specimens before the heating process in order for the documentation of the cooling rate to be possible.
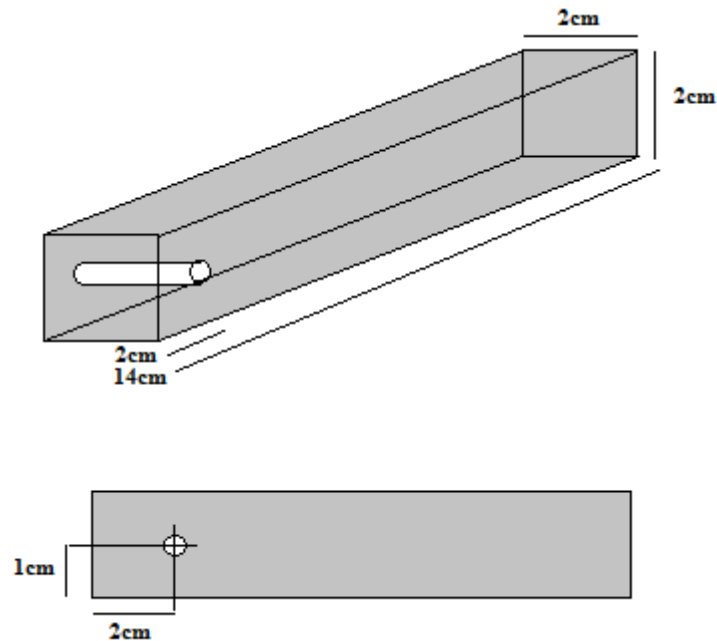
Figure 3: Location of temperature measurement

Three sections of each alloy were initially heated in a furnace to 580C for 8 hours and then left to cool naturally at room temperature. The cooling rate of the specimens can be seen in Fig. 4.
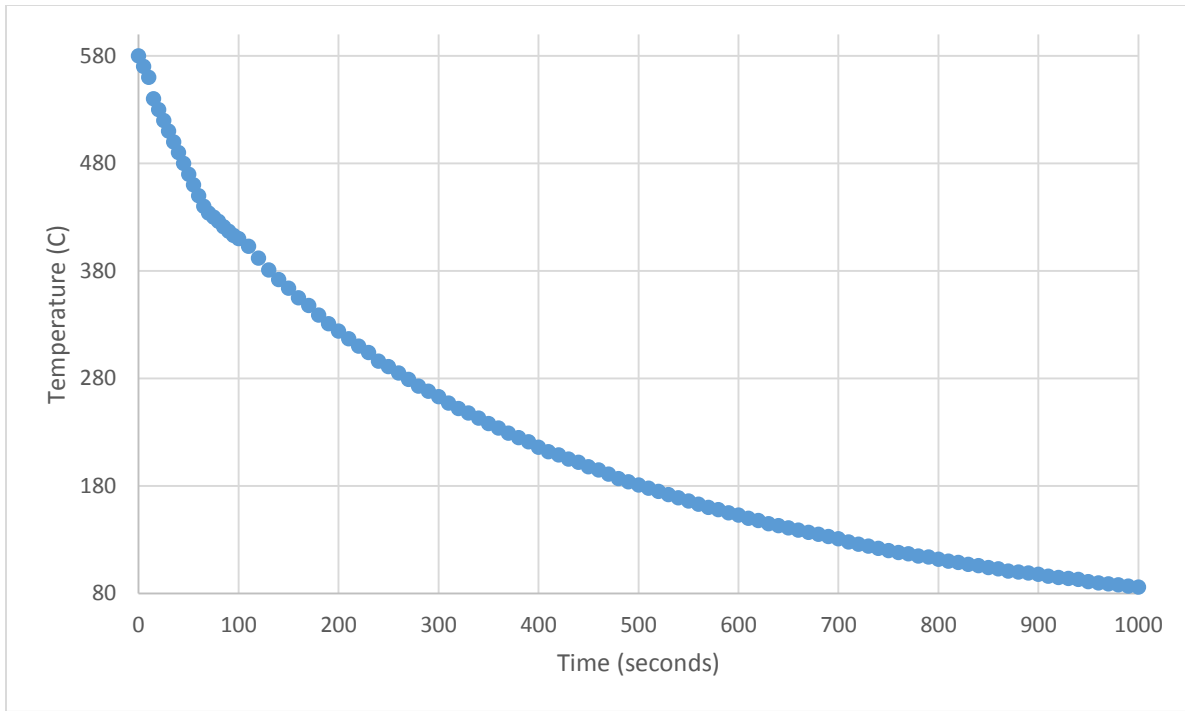
Figure 4: Thermal cycle of the specimens

As soon as the temperature of the specimen reached 80C it was put in a freezer at approximately -18C to prevent ageing. The specimens remained at low temperature until their final processing. The tensile specimens were made according to ASTM E 8M. The final form of the specimens is shown in Fig. 5. The tensile fracture tests were performed by an Instron 8801.
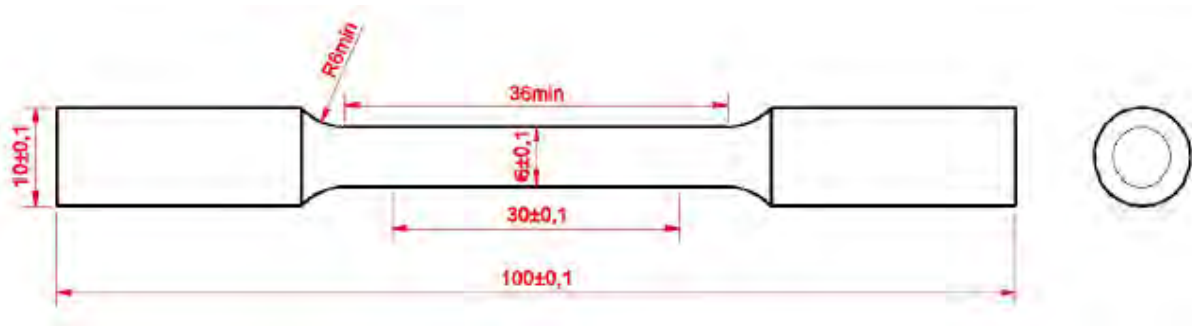

Figure 5: Specimens' dimensions

3.2.3 Tensile Test Results

Through tensile fracture tests, the σyield of the alloys were acquired. The results of the tests are listed in the table below

Alloy	Specimen	σ_{yield} (MPa)	σ_{yield} mean (MPa)	$\varepsilon_{fracture}$ (%)
6005	1st	72	70.33	27.7
	2nd	69		25
	3rd	70		26.3
6063	1st	52	52.33	33.3
	2nd	53		30.5
	3rd	52		30.5
6082	1st	83.75	88.91	16.6
	2nd	90		15.2
	3rd	93		16.6

Table 4: Experimental Results

4. Results and discussion

4.1 Results
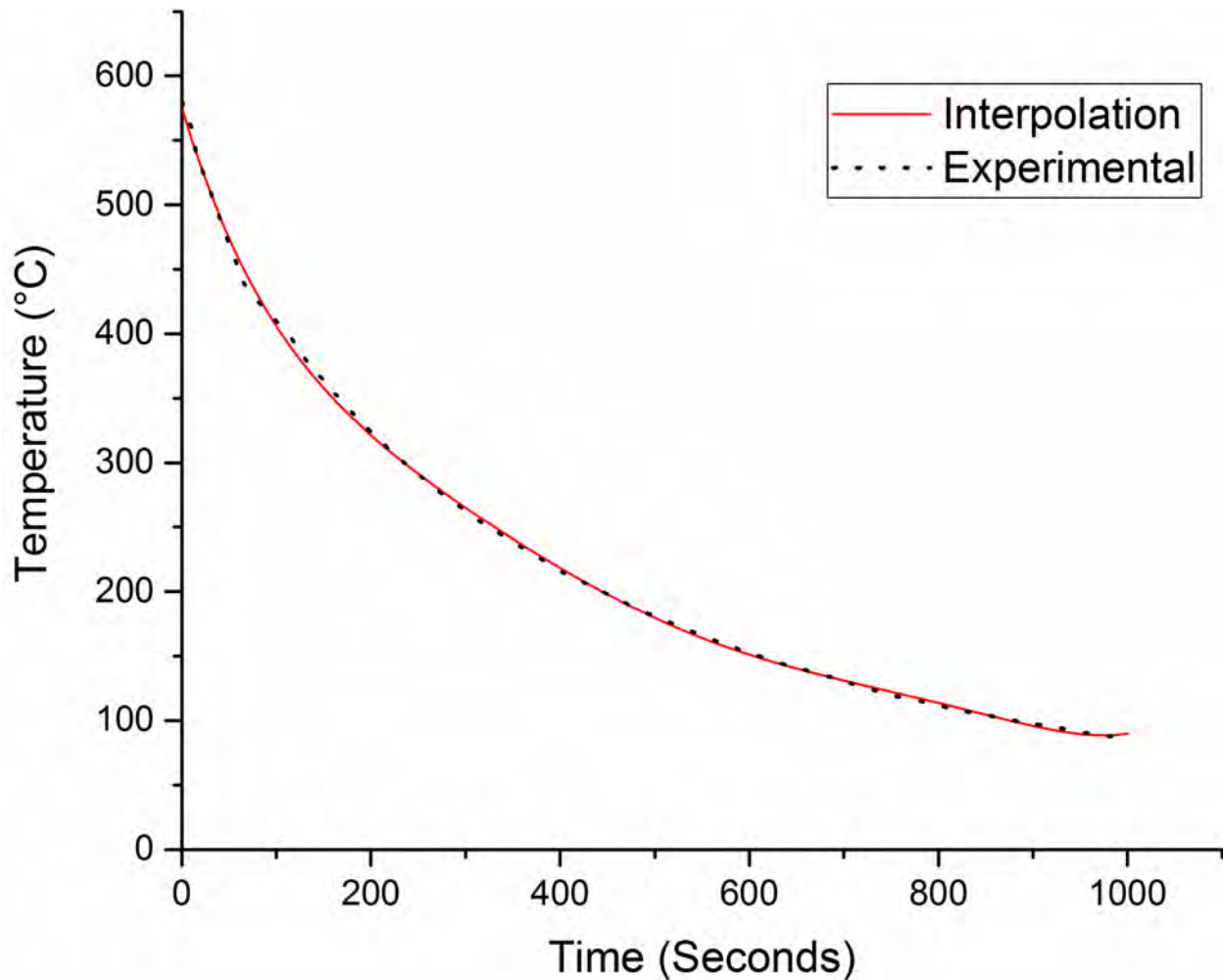
Figure 6: Interpolation of the thermal cycle

The temperature measurements of the cooling process, are shown in Figure 6. The experimental data were fitted with a 6th degree polynomial interpolation. The interpolation's equation is shown below:

T(C)=(9.33036479388425E-15)*(t^6)-(3.10708896200147e-11)*(t^5)+(4.07087591321469E-08)*(t^4)-0.0000268875260317492*(t^3)+0.00988295258716931*(t^2)-2.44895496190384*t+575.206155973486+273.15
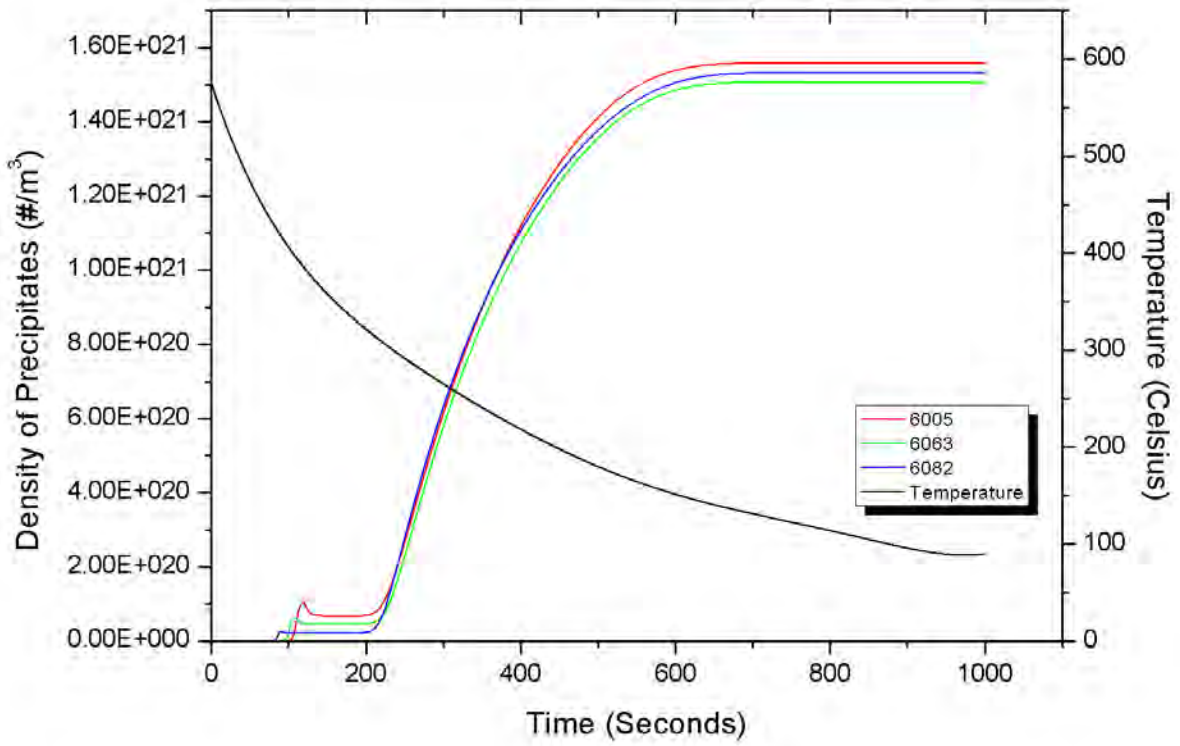
Figure 7: Density of particles

The precipitate density throughout the process, is shown in Figure 7.
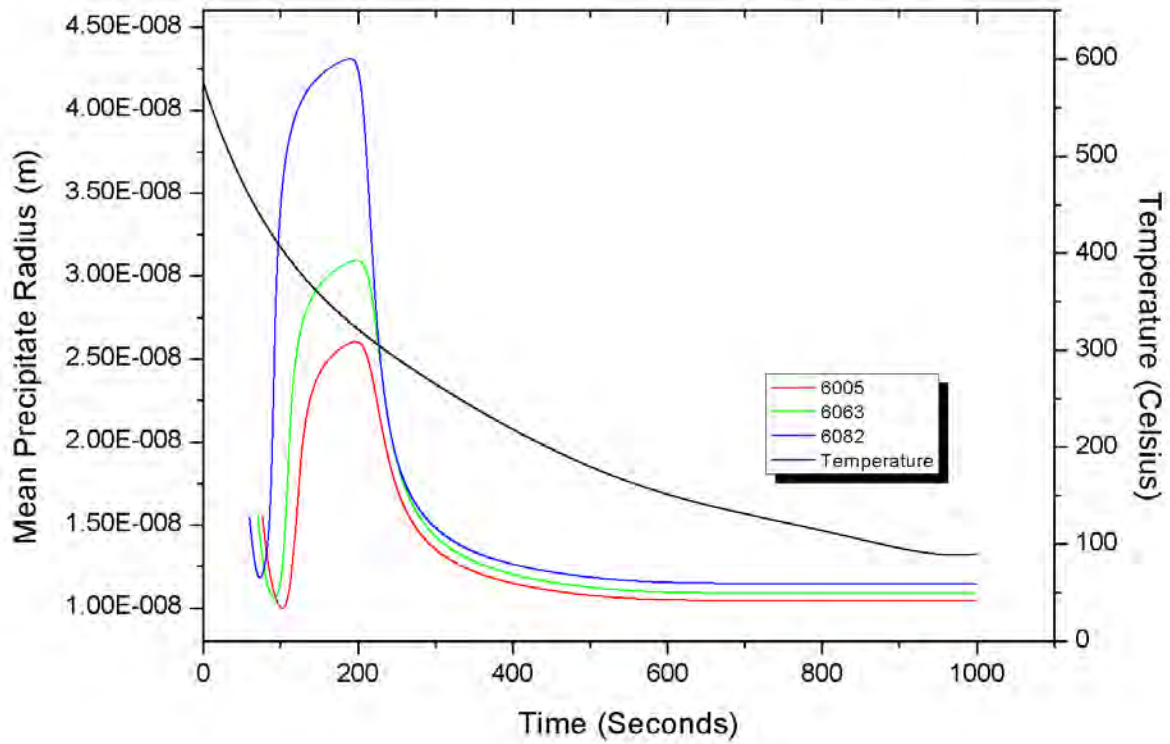
Figure 8: Mean particle radius

The evolution of the mean precipitates' radius, is shown in Figure 8. The radius initially decreases and then begins to increase until it reaches it's maximum value. Then the radius decreases and takes it's final value until the end of the process.
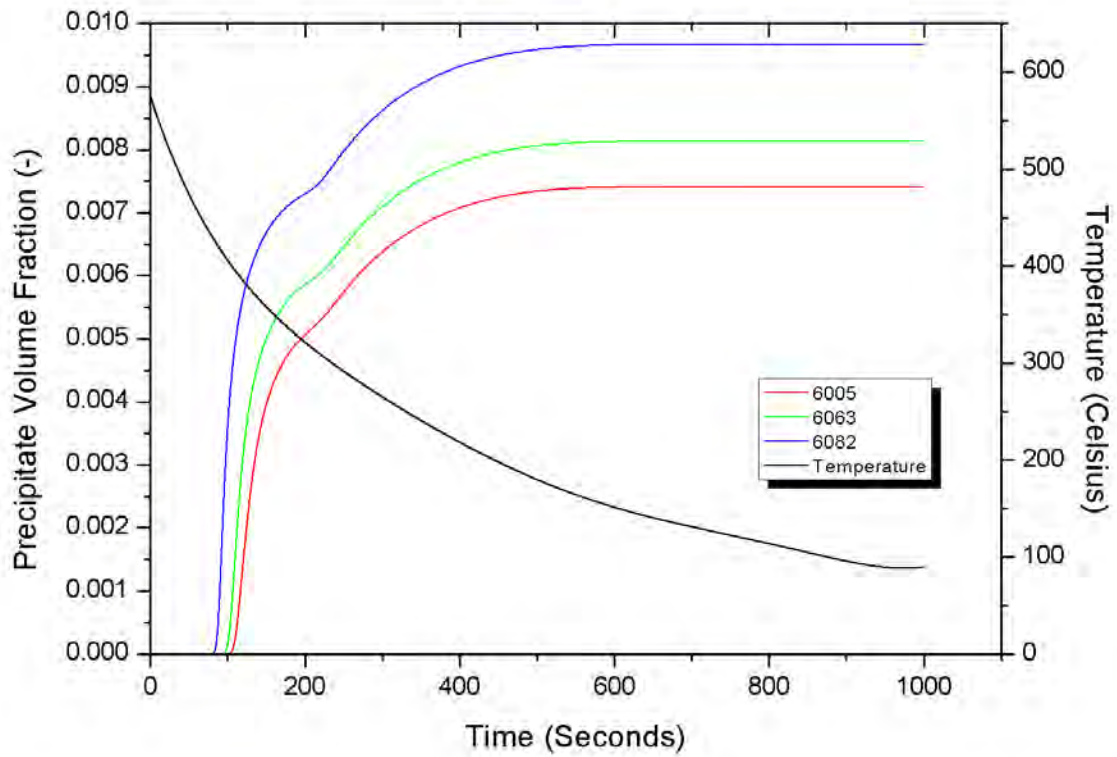
Figure 9: Volume fraction of particles

The evolution of the precipitate Volume fraction, is shown in Figure 9. The volume fraction's rate of increase decreases slightly around 300C but then continues to increase while the temperature is decreasing.
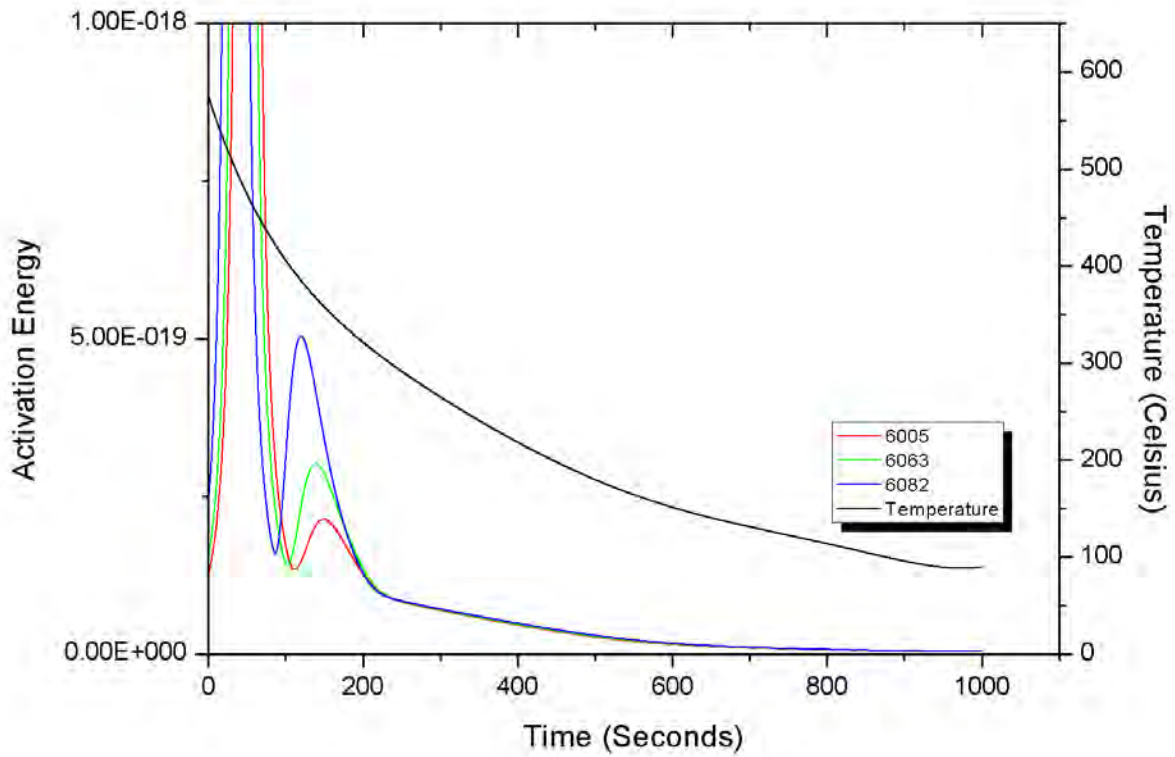
Figure 10: Activation energy

The evolution of the activation energy DGs, is shown in Figure 10. Activation energy, decreases until it reaches it's first minimum around 100-120 sec for all the alloys. Activation energy starts to increase and reaches a local maximum. Then it decreases while the temperature is also decreasing.
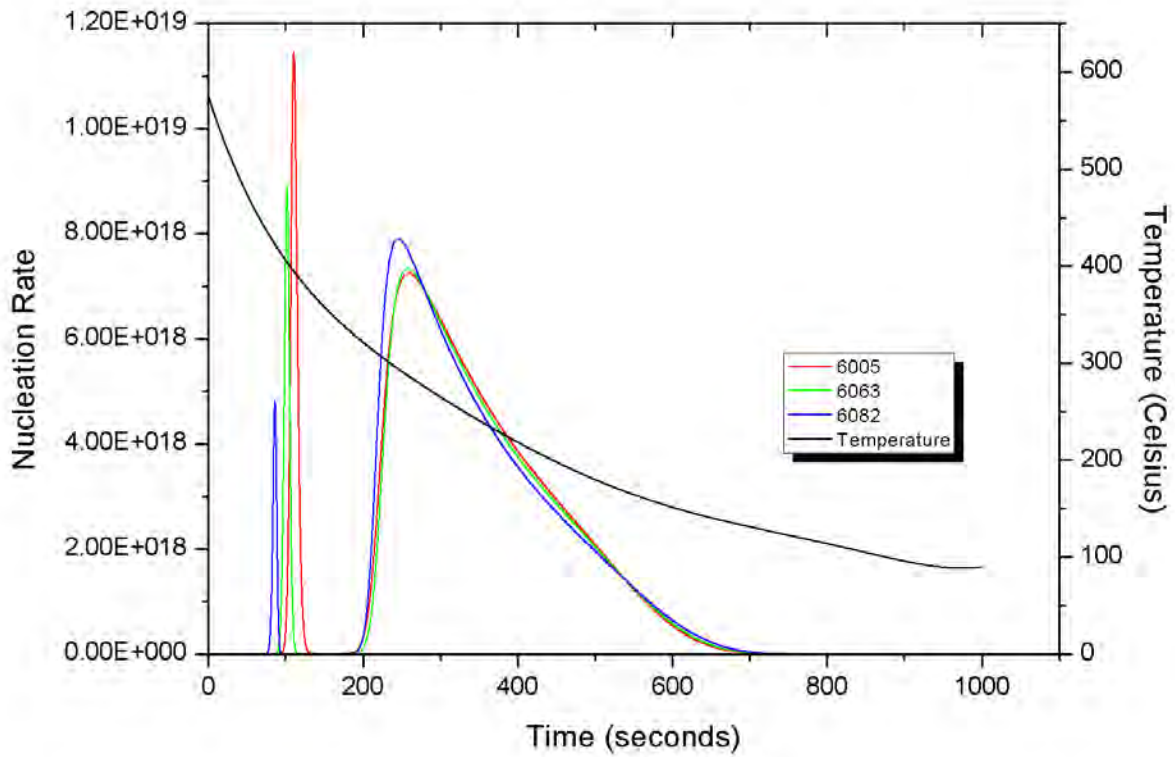
Figure 11: Nucleation rate

Figure 11 shows the nucleation rate throughout the cooling process. It is obvious that two nucleation events occur, a short one and a longer one. The reason why this happens, will be discussed later.
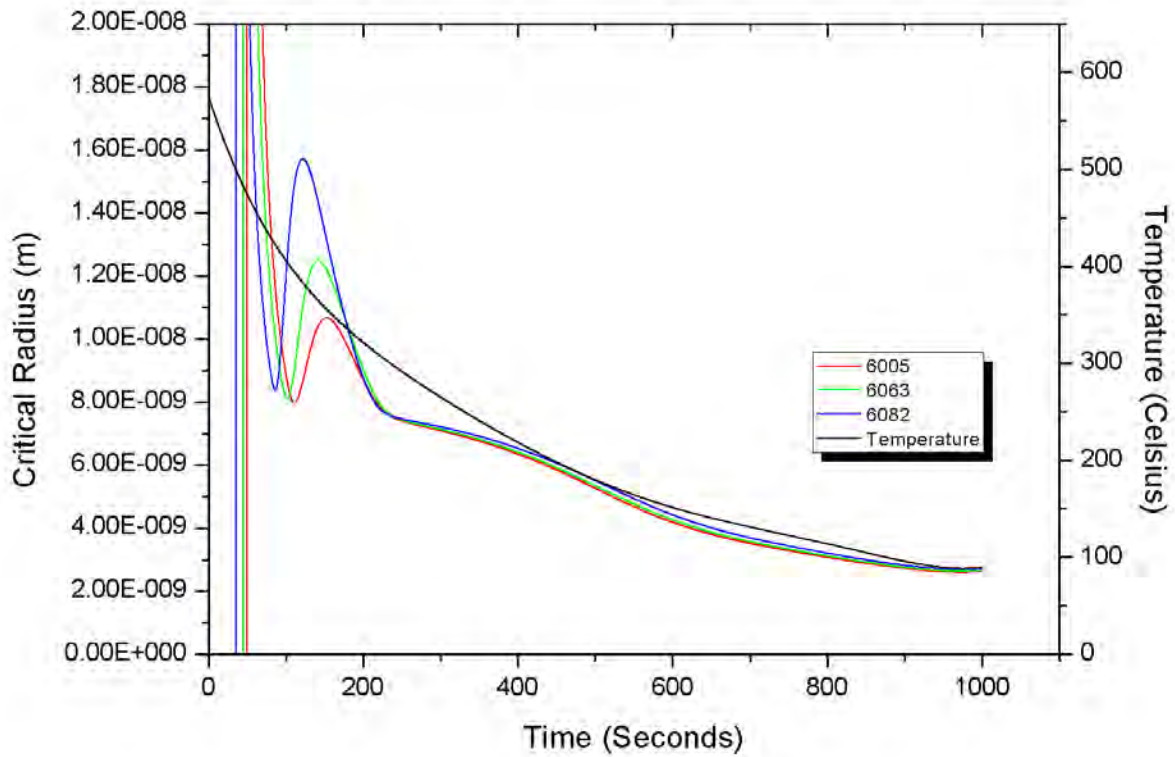
Figure 12: Critical radius

In Figure 12 the critical radius for precipitation is shown. Critical radius follows the same trend as activation energy.
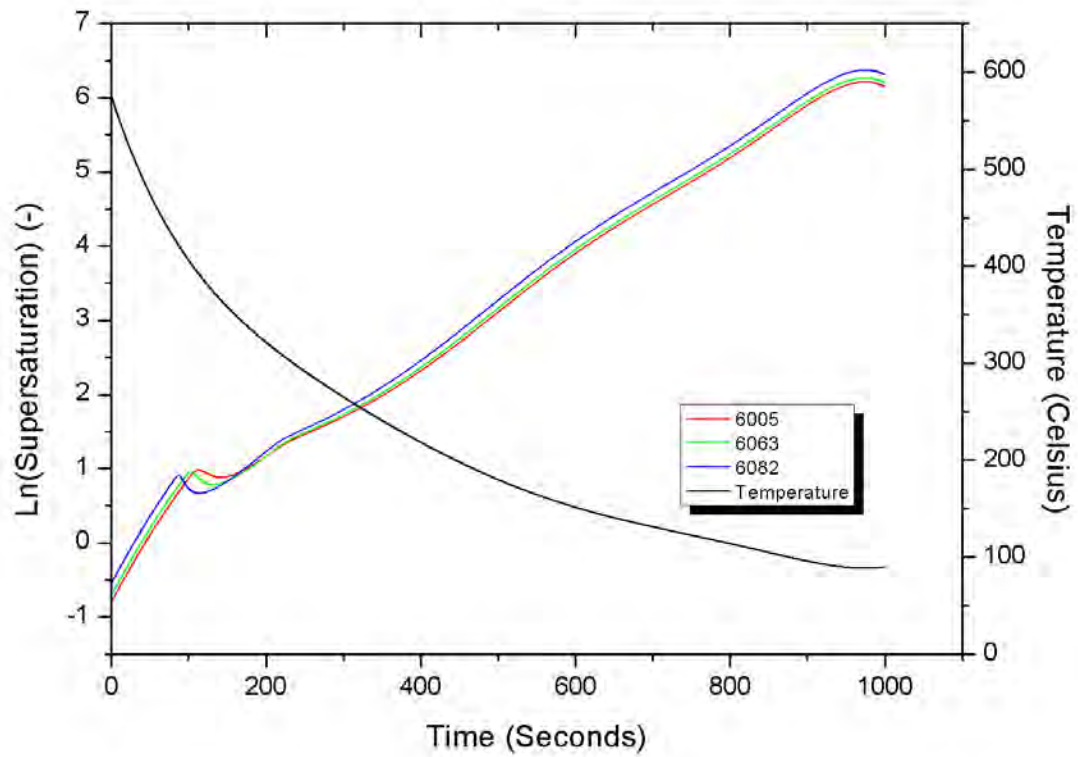
Figure 13: Natural Logarithm of Supersaturation

Figure 13 shows the evolution of the natural logarithm of supersaturation. This parameter has one of the dominant roles in nucleation.
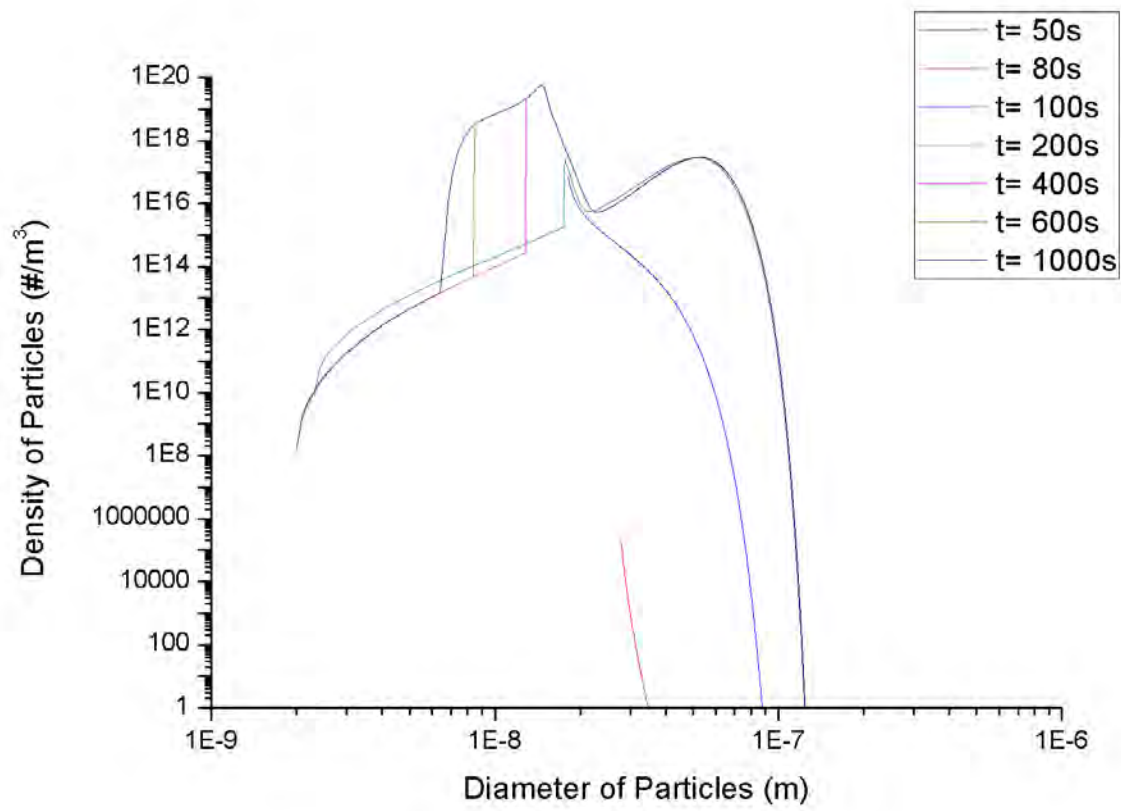
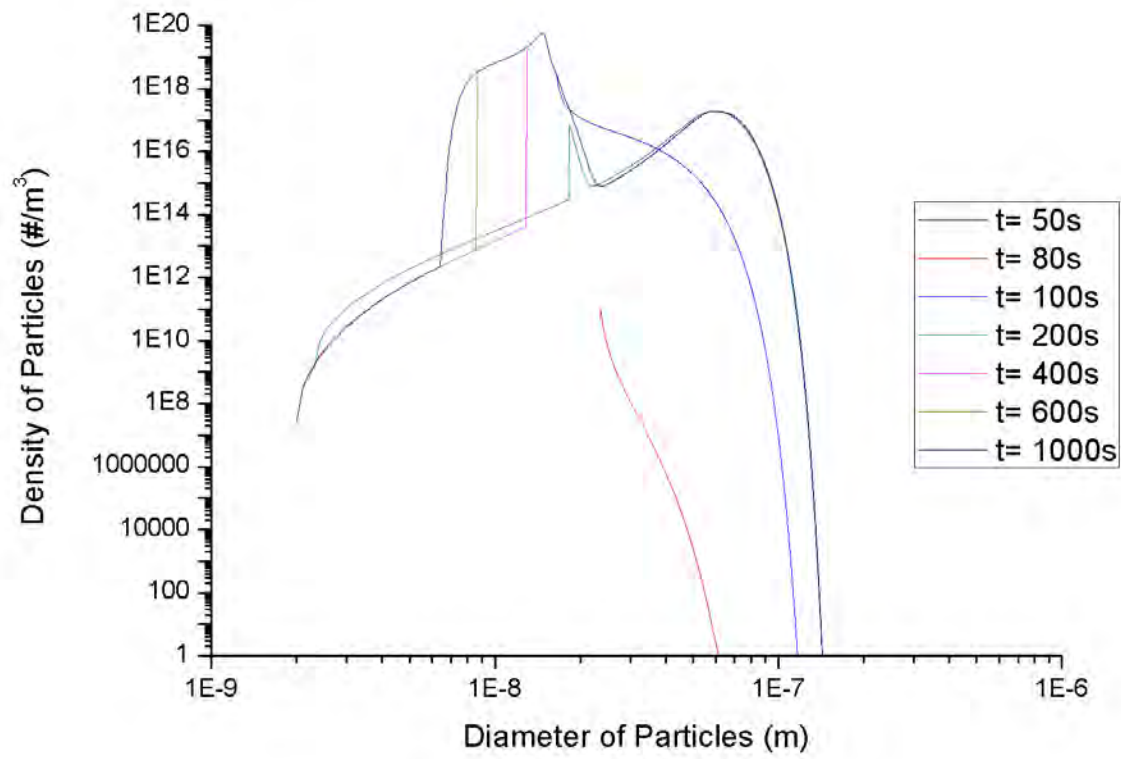*Figure 14: Particle Size Density of 6005 alloy*

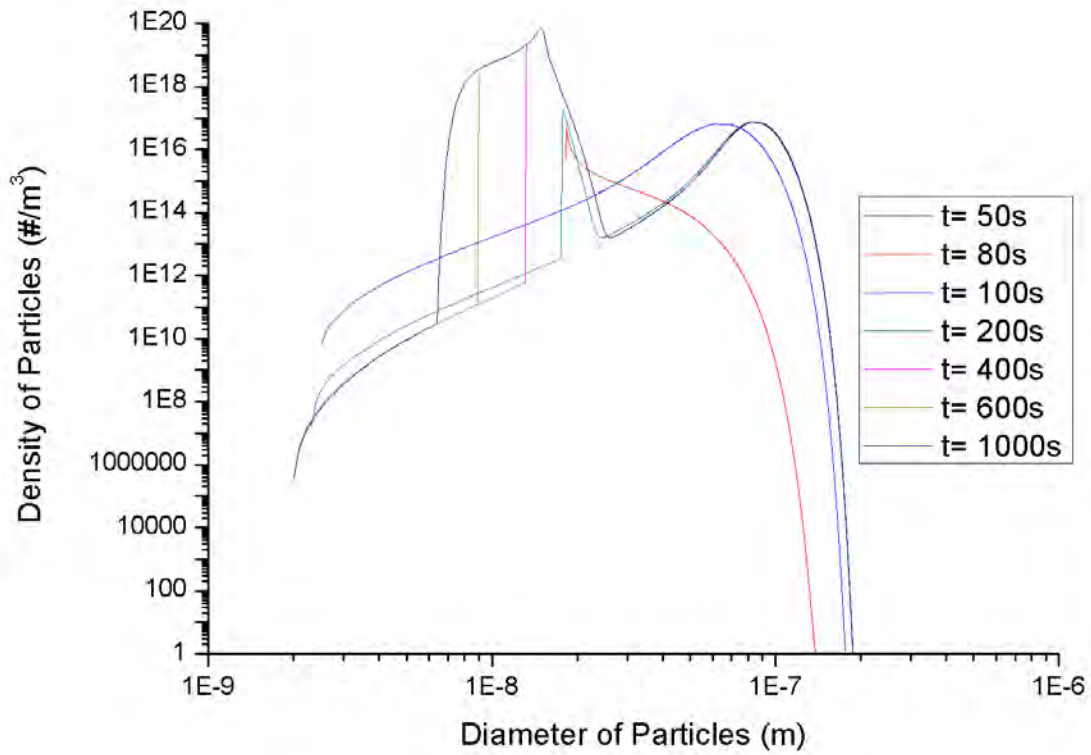*Figure 15: Particle Size Density of 6063 alloy*

Figure 16: Particle Size Density of 6082 alloy

Figures 14, 15 and 16   show the PSD of the three alloys throughout the process. These figures provide a better understanding of the nucleation and growth events throughout the cooling procedure.
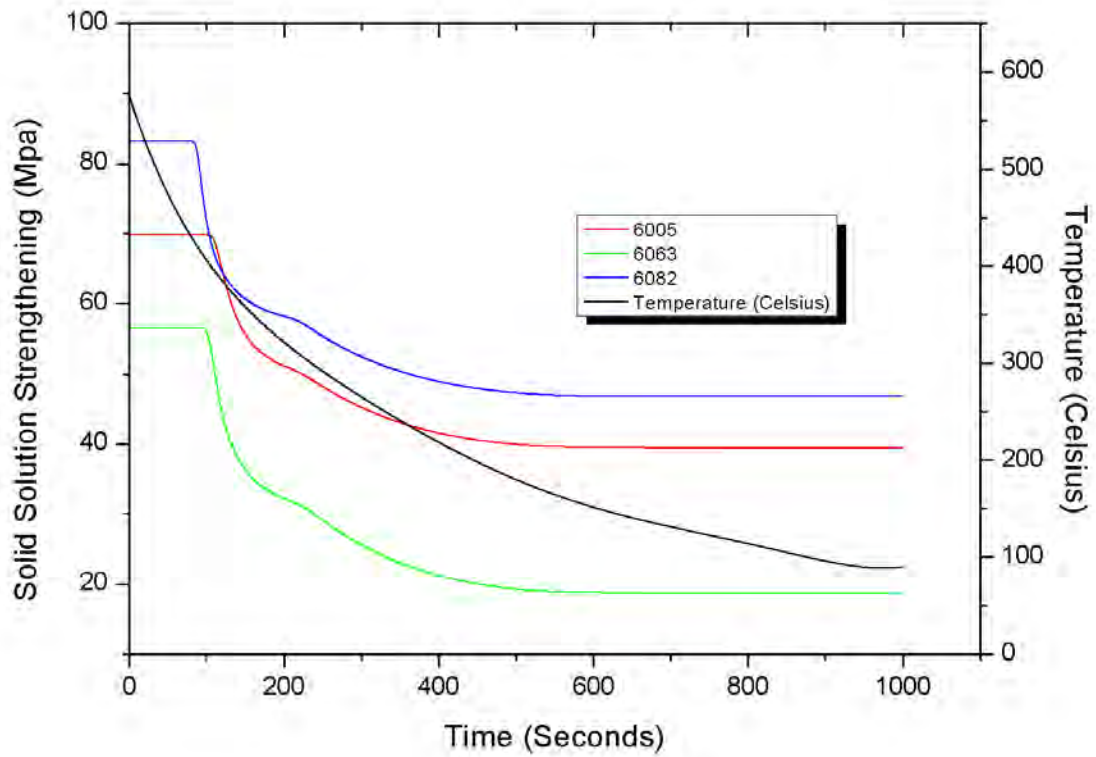
Figure 17: Solid Solution Hardening

In Figure 17 the contribution of solid solution in the overall strengthening of the alloy is shown. Solid solution begins with it's maximum value and then begins to decrease.
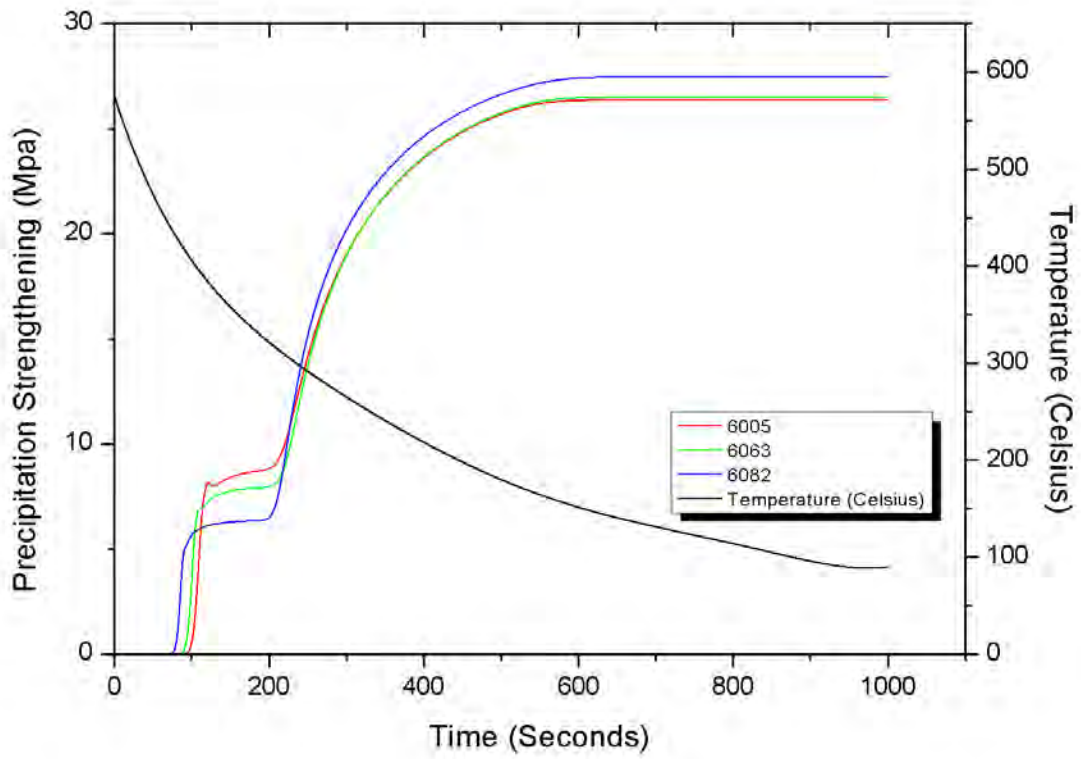
Figure 18: Precipitation Hardening

Figure 18 shows the evolution of precipitation's hardening.
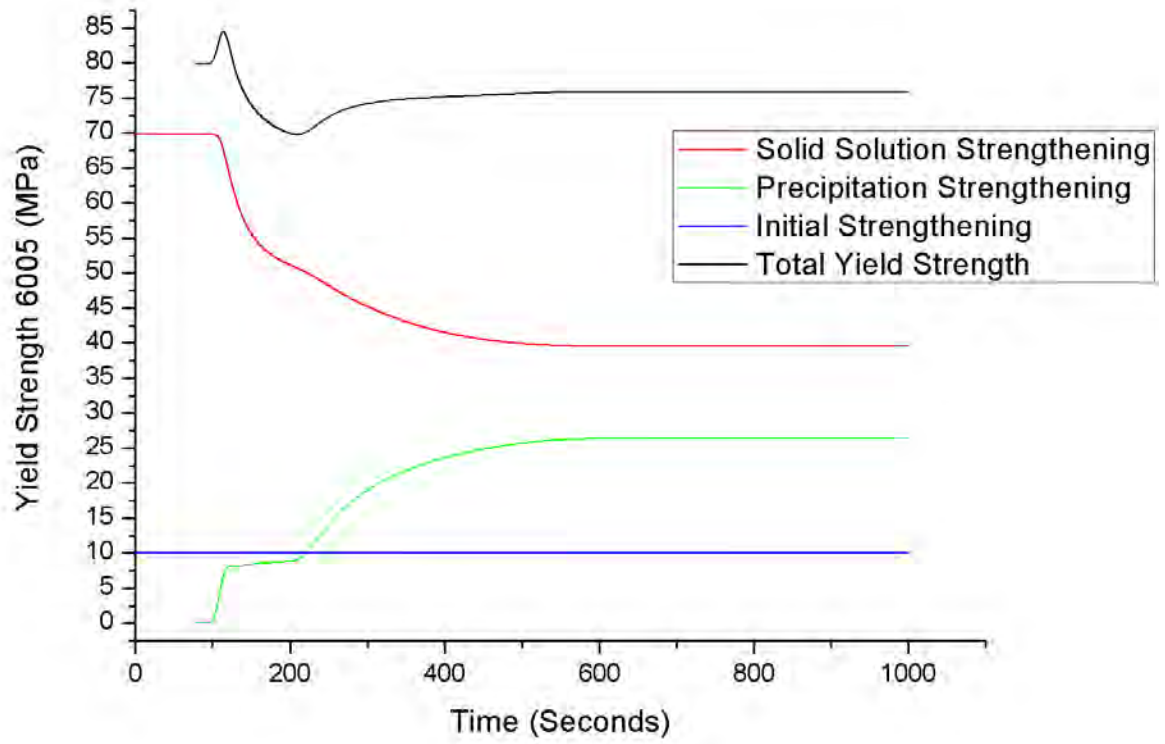
Figure 19: Total hardening of 6005
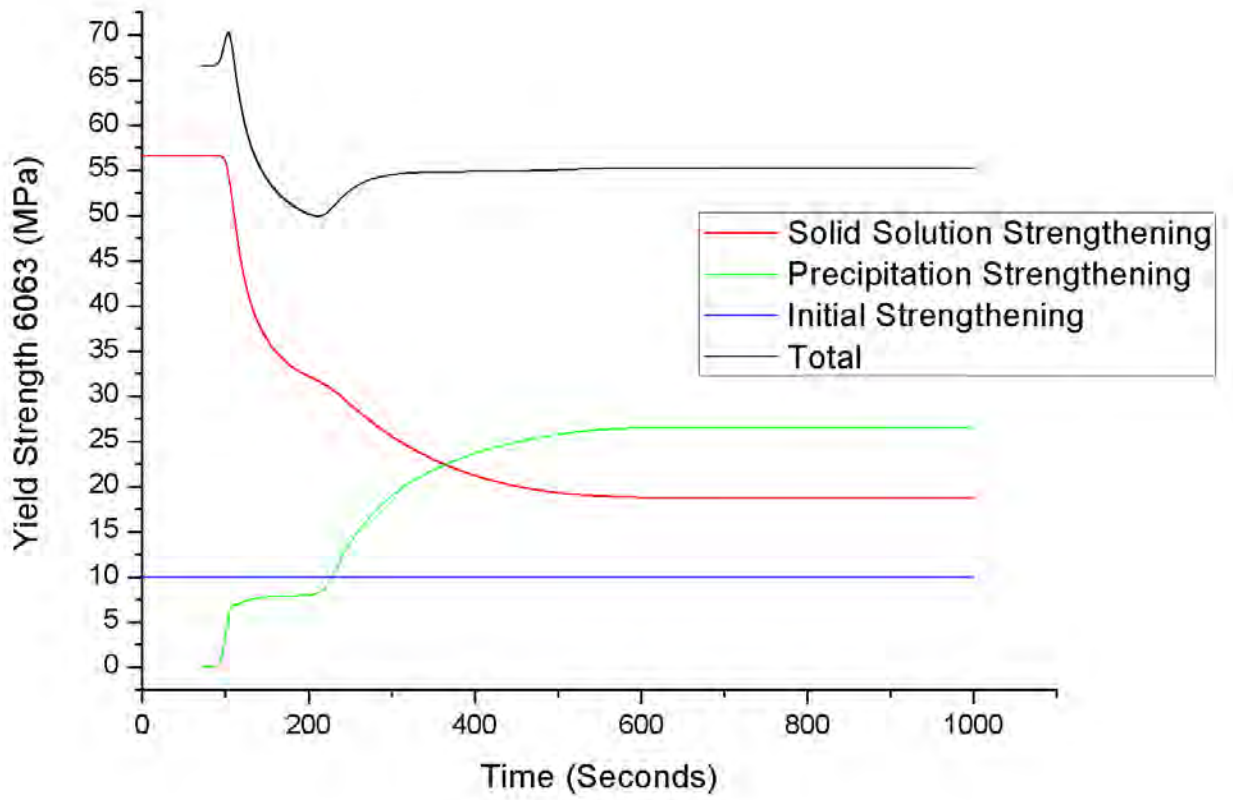
Figure 20: Total hardening of 6063
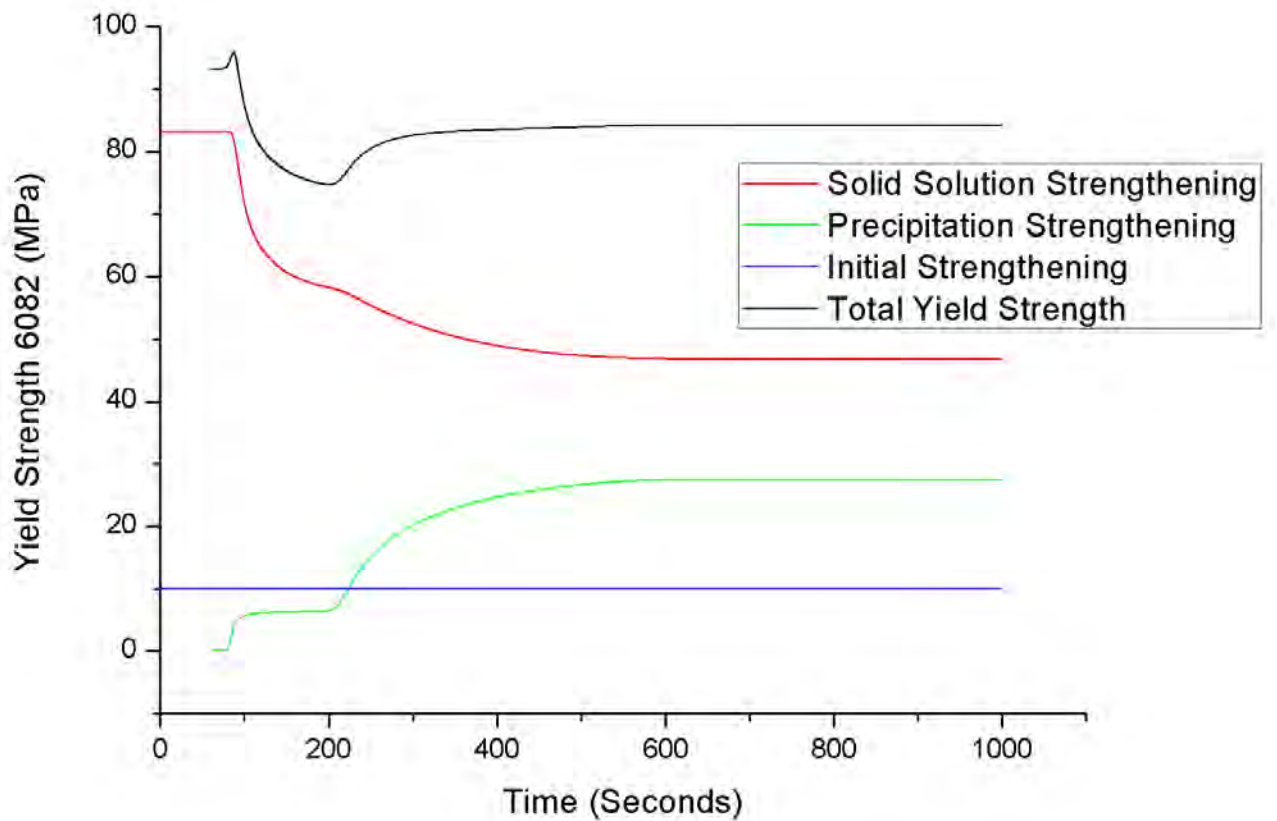
Figure 21: Total hardening of 6082

Figure 19, 20 and 21 show the evolution of the yield strength of the 6005 6063 and 6082 alloy. Solid solution strengthening is shown decreasing as soon as the precipitation strengthening increases. The initial strengthening consists of work hardening, Hall-Petch hardening and lattice resistance hardening.
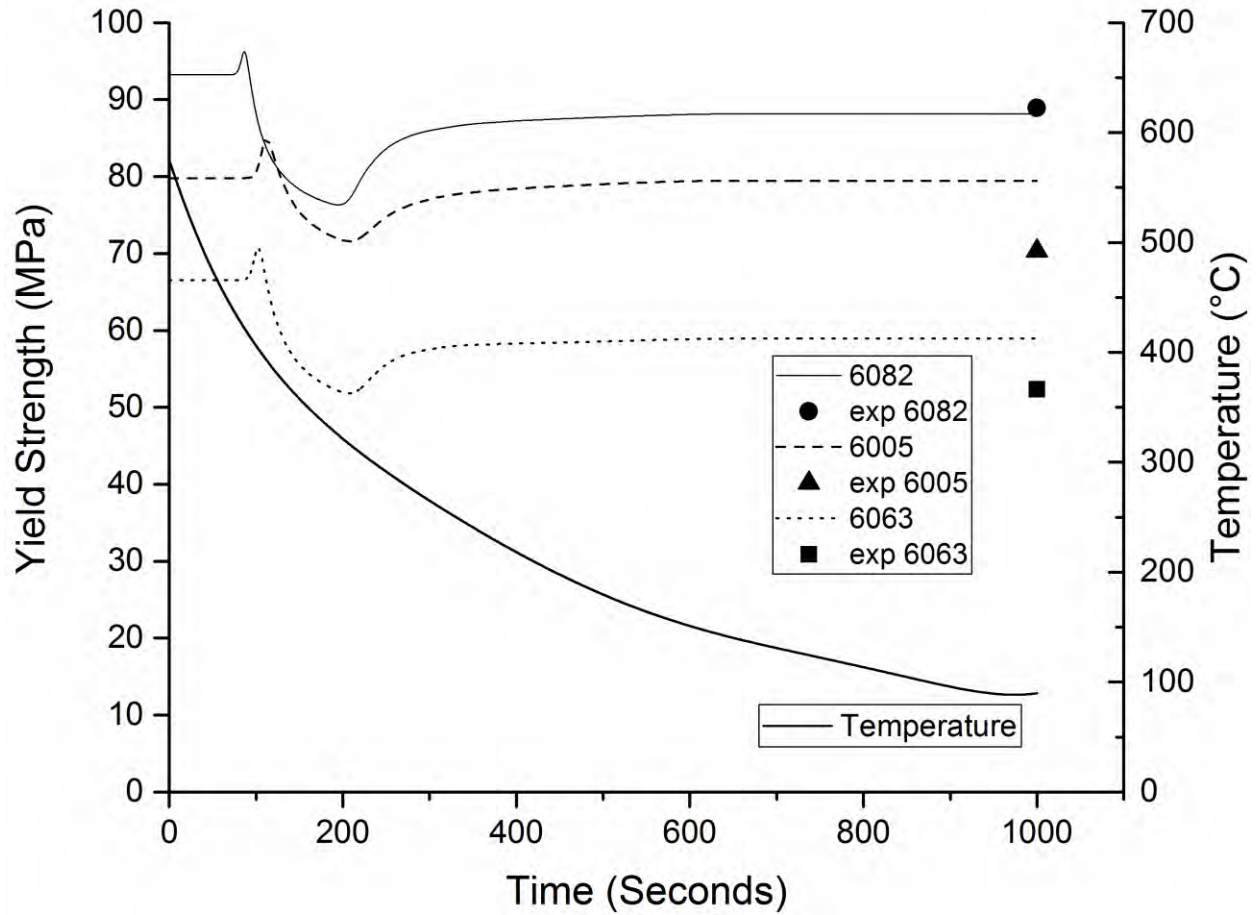
Figure 22: Total hardening comparison of 6005, 6063, 6082

Figure 22 shows the yield strength evolution of all three alloys (6005, 6063, 6082) with respect to Temperature and compares the results of the simulation with the results of the experiments.

4.2 Discussion
(For the 6005 alloy)

4.2.1 Particle Number and Nucleation events

The nucleation events are observed in the Particle Number (Figure 7). At 100sec the first nucleation event begins and the number of particles increases until 120sec where it becomes stable. The second increase occurs when the second nucleation event begins at 200sec and lasts up to about 620sec where it is near it's final value.

4.2.2 Activation Energy (DGs)

Activation energy DGs (Figure 10) depends on supersaturation. As supersaturation increases, DGs drops rapidly. At 100sec the 1st nucleation event starts, causing a slight decrease in supersaturation and a corresponding increase of DGs. At 120 sec the 1st nucleation event ceases and growth of the nucleated particles continues up to 200 sec. Growth in this time period causes a further drop in supersaturation up to 150 sec. However after the 150sec, the drop in temperature dominates and the supersaturation increases again, leading to a decrease of DGs. The 2nd and longer nucleation event commences at 200 sec and lasts up to about 620 sec where the rate drops to zero (DGs=0). This can be seen in the Number of particles figure (Figure 7) where the number rises due to nucleation and stabilizes at 620 sec. The supersaturation continues to increase despite of nucleation, since its temperature dependence is more dominant (Figure 13).

4.2.3 Critical Radius (r_c)

Regarding the r_c diagram (Figure 12), critical radius depends on supersaturation which explains the similarity between the critical radius diagram and the DGs diagram (Figure 10). When the 1st nucleation event starts, the supersaturation decreases which results in an increase of the critical radius. As mentioned before the drop in temperature after the 150sec results in the increase of the supersaturation which leads to a further decrease of the critical radius, much like DGs. This results on the precipitation of the smaller particles after 150sec.

4.2.4 Nucleation Rate (S)

The nucleation rate depends on the activation energy. Another look at the DGs diagram (Figure 10) makes it clear why two different nucleation events take place. At 100 sec DGs decreases below a certain value, due to the temperature controlled increase of Supersaturation, and that

is what makes the 1st nucleation event possible. This event stops when DGs increases above this value at 120sec, caused by the decrease in supersaturation caused by the 1st nucleation event. The second nucleation event begins as soon as DGs drops again below this value at 200sec. The nucleation rate diagram (Figure 11) provides a clearer image, of the time that both nucleation events occur and of their duration. Both events are represented by the two peaks of the diagram although the second one is substantially longer, as mentioned before.

4.2.5 Mean Particle Radius (Rmean)

Regarding the mean particle radius, Rmean (Figure 8), at first decreases due to the decrease of the critical radius (Figure 12). After the 1st nucleation event is completed, the mean particle size increases due to growth, between 100-200 sec. At 200 sec the particles grow to a mean size of 2.5E-8. After the 1st nucleation event the mean size drops due to the formation of new smaller particles from the 2nd nucleation event. The new particles have a continuously decreasing critical radius r_c due to the increase of supersaturation. Due to growth, the rmean is always above the r_c curve. However growth slows down with the drop in temperature. At t=600 sec the 2nd nucleation event stops and no further particles form. The mean radius rmean stabilizes as further growth is not feasible below this temperature due to limited diffusion.

4.2.6 Particle Size Distribution (PSD)

Regarding the PSD figure (Figure 14), at 80sec a few particles have precipitated. As the 1st nucleation event continues, at 100sec more particles of smaller diameters continue to precipitate while the previously precipitated particles grow. At 150sec the 1st nucleation event has finished and the particles continue to grow which results in a relocation of the PSD curve to the right, along with the smaller particles that precipitated earlier. At 200sec the 2nd nucleation event has started which can be seen by the left peak that begins to form at 2E-8 diameter of the PSD. This peak continues to grow and move to the left as the 2nd nucleation event continues, and smaller particles begin to precipitate. This is caused by the constantly decreasing r_c due to the increase of the supersaturation. This can be seen in the Rmean graph (Figure 8) where the mean particle radius continues to decrease. Growth no longer takes place because of the decreased temperature and that is why the curve no longer moves to the right. Smaller particles continue to precipitate even after 700sec in a temperature of 130C (403K) until the cooling procedure comes to an end.

4.2.7 Volume Fraction

Regarding the Volume fraction diagram (Figure 9), at 100sec increases because of the 1st nucleation event and continues to increase as the precipitated particles grow. As the volume fraction continues to grow it comes to a tipping point at 200sec which indicates the beginning of the 2nd nucleation event. Finally the volume fraction of the particles stabilizes at 600sec. This can be seen in the Particle number (Figure 7) and rmean diagram (Figure 8), where at 600sec the total number of particles and their mean radius have stabilized, thus the volume fraction reaches it's final value too. The same conclusions, apply to the other two alloys as well.

4.2.8 Yield strength (σ_{yield})

The σ_{yield} of the alloy, as stated before is a result of five different mechanisms: work hardening σ_{WH}, Hall-Petch hardening σ_{GB}, lattice resistance hardening σ_{I}, solid solution hardening σ_{ss} and precipitation hardening σ_{p}. In the simulation, the first three mechanisms are included in one constant σ_{0} which is determined by literature. In the σ_{yield} diagram (Figure 19), the evolution of all three variables (σ_{0}, σ_{p}, σ_{ss}) can be seen. At first, there is no precipitation hardening as there are no particles precipitated yet. Also solid solution hardening (σ_{ss}) has it's maximum value, because all of the Mg and Si are dissolved into the matrix. At 100sec, when the 1st nucleation event and growth start, σ_{ss} begins to decrease while σ_{p} increases, as the first precipitates begin to form and grow. When the 1st nucleation event seizes at 120sec so does the σ_{p}, but σ_{ss} continues to decrease at a slower rate because of the particles that are still growing. At 200sec the 2nd and longer nucleation event begins. That is the reason why σ_{p} begins to increase again. Also as more alloying elements leave the solid solution in order to produce precipitates, σ_{ss} decreases at a greater rate than before. At 600sec both mechanisms have stabilized and reached their final value. That can be seen in the Particles Number (Figure 7) and Rmean diagrams (Figure 8) too. After 600sec both Particles number and Rmean have been stabilized. This means that no more particles are precipitating and their size remains stable, leading to the final value of σ_{p} and σ_{ss}.

The differences between the σ_{yield} of the alloys can be explained by examining the evolution of the σss and σp separately. As mentioned before nucleation depends on activation energy which depends on supersaturation. The content of Mg in 6005 is lower than the other alloys, with 6082 having the largest amount of Mg. This causes the supersaturation of 6005 to increase slower than the other alloys as the temperature drops, which causes a slower initial decrease of DGs and r_{c}. So the 1st nucleation event begins later than the other alloys. This is the reason why σ_{p} also increases later. Since the 1st nucleation event starts later, the precipitation of particles causes the supersaturation to drop later also. DGs depends on supersaturation, so DGs begins to increase again having reached a minimum value lower than the other alloys. The same happens to r_{c}, as it also depends on supersaturation. This results in a higher Nucleation rate

and a higher number of smaller precipitated particles, as it can be seen in the Nucleation Rate (Figure 11), Particles Number (Figure 7) and r_c diagrams (Figure 12). Consequently, the σ_p that results after the 1st nucleation event, is higher than the other alloys. This changes after the 2nd nucleation event has finished. In the Volume fraction diagram (Figure 9), 6005 has the least Volume fraction of particles, when the cooling procedure ends. This is the reason why, 6005 has the least final σ_p of the alloys. 6063 has the second largest final volume fraction, while 6082 has the highest volume fraction. This results in 6082 having the highest final σ_{pp}, 6063 being second and 6005 last.

4.2.9 Limitations

The results of the model are in good agreement with the experimental data. Although two of the limitations of the model are:

1. The model has many adjustable parameters which require experimental data to be determined. The number of nucleation sites and the precipitation strengthening coefficient are the main factor affecting the results of the simulation.

2. The Mg2Si equilibrium phase, is the only precipitate considered. During cooling, it is likely that metastable phases form with a different strengthening factor than β-phase.

5. Conclusions

In this study the kinetic KWN model and a strengthening model were used in order to predict the yield strength of three aluminum alloys after the homogenization cooling. The conclusions of this study are the following:

- The resulted yield strengths are in good agreement with the experimental results. Also the evolution of the yield strength follows a trend that agrees with the literature.
- The precipitation strengthening was also studied individually for every alloy. As expected, the alloy with the larger content of Magnesium had a higher precipitation strengthening in comparison with the alloys of lower content provided that enough Silicon is available.
- The evolution strengthening of the alloys agrees with the literature. As expected the alloys with the larger content in Magnesium and Silicon showed larger solid solution strengthening both in the beginning and in the end of the cooling treatment.
- The model predicted two nucleation events, which agrees with the literature. This shows that the model can simulate correctly the intermediate conditions as well as the final conditions of the alloys.

6. References

[1] P.I. Sarafoglou Simulation and design of the homogenization process of 6xxx extrudable Aluminum alloys, PhD pp. 62-65

[2] Kemal Deliji, Vanja Asanovi, Dragan Radonji, MTAEC9, 39 (4) (2005)101

[3] Polmear I.J., 'Light Alloys, Metallurgy of the Light Metals', Arnold, (1995)

[4] J. V. Langkruis, Ph.D. Thesis, TUDelft, (2000)

[5] O.Reiso, Ph.D. Thesis, Norwegian Institute of Technology, (1992)

[6] Halfdan Kristoffer Småbråten, Master thesis, Norwegian University of Science and Technology, (2011)

[7] G. M.-Nowotnik, J. Sieniawski, Jour. Mat. Proc. Tech., (2005) 367-372

[8] Kinetics of materials, Book

[9] S.N Samaras, G.N Haidemenopoulos, Jour., Mat., Proc., Techn. 194 (2007), 63–73

[10] Y. Birol, Jour., Mat., Proc. Tech. 148, (2004). 250-258

[11] Y. Birol, Met., Mat., Int. 20 (2014), 727-732

[12] Pikee Priya, David R. Johnson, and Matthew J.M. Krane , Numerical Study of Microstructural Evolution During Homogenization of Al-Si-Mg-Fe-Mn Alloys

[13] G. A. Edwards, K. Stiller, G. L. Dunlop and M. J. Couper. The precipitation sequence in MgAlSi Alloys

[14] Slyozov, Lifshitz. The kinetics of precipitation from supersaturated solid solutions. J. Phys.Chem. Solids. 1961, Vol. 19, pp. 39-50

[15] R, Wagner R and Kampmann. Materials Science and Technology. 1991, Vol. 5

[16] Myhr O R, Grong O and Andersen S J. Modelling of the age hardening behavior of Al–Mg–Si Alloys. Acta Materialia. 2001, 49, pp. 65-75

[17] R, Myhr O. Modelling of the microstructure and strength evolution in Al–Mg–Si alloys during multistage thermal processing. Acta Materialia. 2003

[18] O, Myhr O R and Grong. Modelling of non-isothermal transformations in alloys containing a particle distribution. Acta Materialia. 1990, 48, pp. 1605-20

[19] Prangnell, P Robson J D and. Modelling Al3Zr dispersoid precipitation in multicomponent aluminium alloys. Mater. Sci. Eng. 2003, Vol. A, 342, pp. 240-50

[20] Robson, J.D. Modelling the overlap of nucleation, growth and coarsening during precipitation. Acta Materialia. 2004, 52, pp. 4669-76

[21] D. Carron, P. Bastid, Y. Yin, R.G. Faulkner. Modelling of precipitation during friction stir welding of an Al-Mg-Si alloy. TECHNISCHE MECHANIK (2010). 30, pp. 29- 44

[22] S, Hulburt H M and Katz. Some problems in particle technology—a statistical mechanical formulation. Chem. Eng. Sci. 1964, Vol. 23, pp. 68-86

[23] D., RAmkrishna. The status of polulation balances. Reviews in chemical engineering. 1985, 3, pp. 49-95

[24] Aaronson.I, Lee.K. Mechanisms of diffusional phase transformations in metals and Alloys. s.l. : CRC Press

[25] J, Crank. Mathematics of Diffusion. s.l. : Oxford university Press, 2nd edition

[26] Hounslow M J, Ryall R L and Marshall V R. A discretized population balance for nucleation, growth, and aggregation. AIChE J. 1988

[27] W, Martin J. Precipitation Hardening. s.l. : (Oxford: Butterworth-Heinemann), 1998. 2nd

[28] M.F, Shercliff H.R Ashby. A Process Model for Age Hardening of Aluminum Alloys. Acta Metallurgica. 1990, 38, pp. 1789-1802

[29] Y, Deschamps A and Brechet. Influence of predeformation and ageing of an Al–Zn–Mg alloy:II. Modeling of precipitation kinetics and yield stress. Acta Materelia. 1999, 47, pp. 293-305

[30] E. Scheil, Anlaufzeit der Austenitumwandlung, Arch. Eisenhuttenwes. 12 (1935) 564–567